

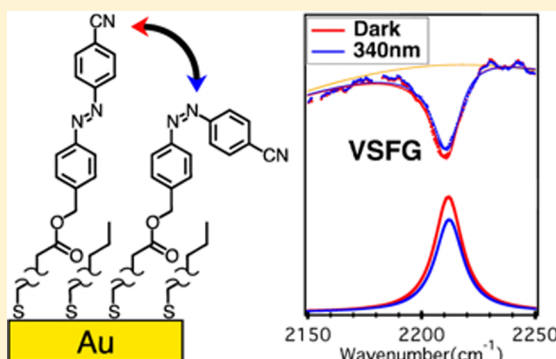
Steric Hindrance of Photoswitching in Self-Assembled Monolayers of Azobenzene and Alkane Thiols

David T. Valley, Matthew Onstott, Sergey Malyk, and Alexander V. Benderskii*

Department of Chemistry, University of Southern California, Los Angeles, California 90089, United States

Supporting Information

ABSTRACT: Surface-bound azobenzenes exhibit reversible photo-switching via trans–cis photoisomerization and have been proposed for a variety of applications such as photowritable optical media, liquid crystal displays, molecular electronics, and smart wetting surfaces. We report a novel synthetic route using simple protection chemistry to form azobenzene-functionalized SAMs on gold and present a mechanistic study of the molecular order, orientation, and conformation in these self-assembled monolayers (SAMs). We use vibrational sum-frequency generation (VSFG) to characterize their vibrational modes, molecular orientation, and photoisomerization kinetics. Trans–cis conformational change of azobenzene leads to the change in the orientation of the nitrile marker group detected by VSFG. Mixed SAMs of azobenzene and alkane thiols are used to investigate the steric hindrance effects. While 100% azobenzene SAMs do not exhibit photoisomerization due to tight packing, we observe reversible switching (>10 cycles) in mixed SAMs with only 34% and 50% of alkane thiol spacers.



INTRODUCTION

A class of versatile photoswitchable molecular devices is based on surface functionalization with azobenzenes.¹ Incident light induces reversible switching between the trans and the cis conformations of the azobenzene. Light-induced changes on azobenzene monolayers have been applied to a variety of devices including optical information storage,² controllable wettable surfaces,^{3,4} liquid crystal alignment,⁵ and molecular electronic switches.^{6–9} These applications all rely on the electrical, mechanical, or optical property changes upon isomerization between the cis and the trans isomers of the azobenzene. The ultimate performance of the devices is dependent on a number of factors that affect isomerization such as stability, transition times and doses, and monolayer formation.¹⁰ To improve these photoactive surfaces and devices, it is first important to characterize the molecular organization and understand critical factors affecting isomerization such as packing, steric effects, and transition kinetics.

One widely utilized method of functionalizing a surface with azobenzene is to form a self-assembled monolayer (SAM) on a gold surface by chemisorption of a molecule with a thiol headgroup and azobenzene-functionalized tail.^{8,11–14} The strong gold–thiolate bonds allow for high-density, aligned monolayers to form well-controlled surfaces.¹¹ Although not the only method of functionalizing a surface with azobenzene,^{4,15} gold–thiol SAMs allow for a uniquely robust method of coating a gold surface^{11,16} or nanoparticle^{14,17} with a variety of molecules. Specifically, for binary SAMs (SAMs composed of two chemical constituents), there has been a great deal of studies looking at the preferential coadsorptive properties,¹⁸

phase separation,^{19,20} effects of composition on morphology,^{21,22} and relative device performance¹⁹ using a variety of methods including surface wetting angle,^{18,20} STM,^{8,9,21,23} reflection IR,²⁰ and XPS.^{21,22,24,25} Binary SAMs with an azobenzene-functionalized component have been built with an additional spacer component for chemical diversity of the device,^{15,26,27} to pair the chemical functionalization of a second group to that of the azobenzene,^{28,29} as well as to free up hindered isomerization from the neat azobenzene films.^{26,30,31} In this study we are looking to get a molecular picture of the azobenzene isomerization in these binary monolayers that guide macroscopic device performance.

Vibrational sum-frequency generation (VSFG) is a surface-selective spectroscopic technique that has previously been shown to yield detailed information on molecular organization such as chemical structure,³² packing,^{33–35} orientation,^{35–37} conformation,^{33,38–42} and ultrafast dynamics^{43,44} in molecular monolayers on surfaces. These properties make it an appropriate tool to characterize the surface coverage and molecular orientation of azobenzene-containing SAMs. There has been a limited number of papers which have utilized VSFG to characterize the isomerization of azobenzene in monolayers at the air–water interface^{45–48} and only one report on azobenzene-containing adamantane SAM on gold.⁴⁹

In this paper we present a novel synthesis using simple protection chemistry to synthesize an azobenzene-function-

Received: June 6, 2013

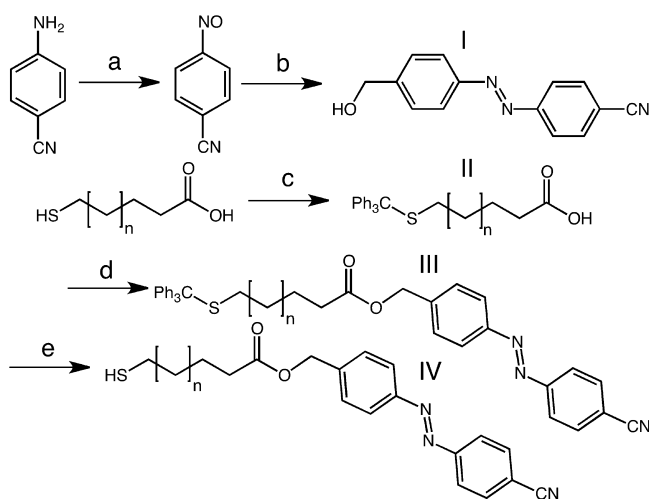
Revised: August 2, 2013

alized alkane thiol molecule which can be used to form SAMs that either are 100% functionalized with azobenzene or contain a mixture of azobenzene-functionalized thiols and simple alkane thiol 'spacers'. We then use VSFG to characterize the spectra of the monolayers and quantitatively determine the relative concentrations of azobenzene-functionalized thiol to alkane thiol spacer. VSFG orientational analysis is applied to investigate the mechanism of isomerization. We demonstrate that isomerization is effectively arrested by steric hindrance in 100% azobenzene monolayers but proceeds readily when the azobenzene groups are separated by the spacers.

EXPERIMENTAL SECTION

Synthesis. Synthesis of the azobenzene-functionalized thiol is accomplished in four steps (Scheme 1). First, we synthesize the

Scheme 1. Synthetic Scheme for the Azobenzene-Functionalized Alkane Thiol^a



^a(a) Oxidation of 4-aminobenzonitrile with 2 equiv of oxone (52%). (b) Addition of 1 equiv of 4-aminobenzoalcohol (36%). (c) Protection of 15-mercaptopentadecanoic acid with trityl chloride (67%). (d) Esterization between protected thiol and product I. (e) Deprotection with trifluoroacetic acid (65% yield for d and e).

alcohol and nitrile-functionalized azobenzene (I) from precursors 4-aminobenzonitrile and 4-aminobenzoalcohol.^{15,50} Second, the thiol group on the linker molecule 15-mercaptodecanoic acid is protected with triphenylmethyl chloride (II).⁵¹ Third, the protected linker and azobenzene are esterized (III).¹⁵ Finally a deprotection step yields the product (IV).

Synthetic construction of the molecule is such that the nitrile group on the azobenzene moiety acts as a convenient vibrational chromophore, a spectroscopic marker which would change its orientation with respect to the plane of the substrate upon photoisomerization. Because of the high affinity of the thiol group for the gold surface, SAMs of binary composition can be formed by incubating a clean gold substrate in a mixed solution of the azobenzene-functionalized thiol with dodecane thiol in ethanol at various ratios while the total concentration of both thiols is 1 mM.¹¹

Synthesis of 4-(4-(Hydroxymethyl)phenyl)diazenylbenzonitrile. 4-Aminobenzonitrile(g) (Aldrich, 98%) was dissolved in 10 mL of dichloromethane and stirred with 2 equiv of oxone in 45 mL of water for 3 h at room temperature under N₂. The solution was extracted with dichloromethane (DCM) twice, and the organic phase was washed with 1 M hydrochloric acid, saturated bicarbonate solution, water, and brine. DCM was then evaporated under vacuum, resulting in 76% yield of 4-nitrosobenzonitrile. 4-Nitrosobenzonitrile and 4-aminobenzoalcohol (Aldrich, 98%) were

then dissolved at a 1.2:1 molar ratio in 50 mL of acetic acid and stirred under N₂ for 3 days. The solid product (I) was filtered, washed with water, dried, and recrystallized in ethyl acetate (EtOAc) resulting in 36% yield product.

Protection, Esterization, and Deprotection. 15-Mercaptopentadecanoic acid (Aldrich, 97%) and triphenylmethyl chloride (Alfa Aesar, 98%) were dissolved in 8 mL of *N,N*-dimethylformamide (DMF) and stirred under N₂ for 6 h. A 50 mL amount of water was added, the solution was extracted with ethyl acetate and washed with water and brine, and the solvent was evaporated under vacuum, resulting in product II with 67% yield. In 50 mL of 3:2 acetonitrile:DMF, 1 mol equiv of compound I, compound II, 1*H*-benzotriazolium 1-(bis(dimethylamino)methylene)-5-chloro-, hexafluorophosphate (1-),3-oxide (HCTU, Fluka, 98%), 4-dimethylaminopyridine (DMAP, Alfa Aesar, 99%) were combined. *N,N*-Diisopropylethylamine (DIEA, Sigma-Aldrich, 99%) was added, and the solution was stirred under N₂ for 24 h. The resultant solid (III) was filtered, washed with acetonitrile, redissolved in DCM, and dried under vacuum. Deprotection was performed by adding 1 mL of trifluoroacetic acid to 0.2 g of compound III at 0 °C. A 100 μL amount of triisopropylsilane was added dropwise. The solution was stirred for 10 min and dried under vacuum. The resultant product IV with 65% yield was purified using EtOAc/hexanes column chromatography.

Formation of SAMs. Solutions were prepared of mixtures of compound IV and 1-dodecanethiol of 1 mM total concentration in absolute ethanol. Gold substrates were cleaned with hot, fresh piranha solution (4:1 H₂SO₄:H₂O₂) for 15 min and sonicated in ethanol for 2 min. The gold substrate was placed in solution for 24 h for SAM formation. Afterward, the substrate was rinsed with ethanol and dried with N₂.

Spectroscopy. Our broad-band vibrational SFG (BB-SFG) spectroscopy setup is based on a femtosecond Ti:Sapphire laser system (Spectra Physics Spitfire) retrofitted with a Coherent Legend regen cavity, which is pumped with a Nd:YLF laser (Evolution-30, Spectra Physics) and seeded with a Ti:Sapphire oscillator (Kapteyn-Murnane Laboratories) centered at ~800 nm (full width at half-maximum, fwhm ≈ 50 nm). Sixty percent of the uncompressed fundamental output of the amplifier (4 mJ per pulse at 1 kHz repetition rate) is sent through a compressor producing ~60 fs pulses (1.8 mJ, ~796 nm, fwhm ≈ 27 nm) and used to pump an optical parametric amplifier (TOPAS-C, Light Conversion). The signal and idler pulses (λ = 1.1–2.6 μm) produced from the TOPAS are mixed in a difference frequency generator (NDFG, Light Conversion) to yield tunable infrared (IR) pulses (500–4000 cm⁻¹). We are able to obtain 10 mW of IR centered at either 2900 (C–H stretch region) or 2200 cm⁻¹ (C–N stretch region) with fwhm ≈ 350 cm⁻¹. The remaining 40% of the uncompressed fundamental pulse was directed into a second compressor to produce 60 fs visible pulses, which were then sent into a high-power air-spaced etalon (TecOptics; fwhm = 17 cm⁻¹, free spectral range ≈ 480 cm⁻¹, and finesse ≈ 65) at 11° incidence angle from the surface normal to produce picosecond narrow-bandwidth pulses. IR and visible pulses were focused onto the sample surface by a 25 cm focal length CaF₂ lens and 45 cm BK7 lens, respectively, to a spot size of 150 μm. Incidence angles of the visible and IR beams are α₁ = 63° and α₂ = 66° from surface normal, respectively. The laser power at the sample was 8–9 μJ per pulse for IR and up to 20–22 μJ per pulse for the visible at a 1 kHz repetition rate. The SFG signal was recollimated, spatially and frequency filtered, focused onto the entrance slit of a 300 mm monochromator (Acton Spectra-Pro 300i), and detected using a liquid nitrogen-cooled CCD (Princeton Instruments, Spec-10:100B, 1340 × 100 pixels). We used PPP (SFG-visible-IR), SSP, and SPS polarizations for the experiments. Polarization of the visible beam is controlled using a zero-order quartz half-wave plate (800 nm, CVI Melles Griot), while IR beam polarization was controlled using a zero-order MgF₂ half-wave plate (150–6500 nm, Alphalas), and the SFG polarization was controlled using a zero-order quartz half-wave plate (670 nm, CVI Melles Griot). To eliminate polarization contamination, we used a wire-grid polarizer (Specac) for the IR beam and a polarizing beam splitter cube (Newport) for the SFG beam.

Spectra of the narrow-band visible and broad-band IR pulses were recorded using the same signal collection optics and the same monochromator by replacing the sample surface with a gold substrate (BioGold Microarray Slides, Thermo Scientific). Spectra of the narrow-bandwidth visible pulse were recorded using the same grating and CCD as for SFG detection. Spectra of the IR pulses were measured using an IR grating blazed at 5 μm and a liquid nitrogen-cooled mercury cadmium telluride detector (IR Associates). For all experiments presented here, the time delay between the visible and the IR pulses was set to maximize nonresonant SFG signal. Data was taken also with a delay between the visible and the IR pulses for reduction of nonresonant signal; however, this method reduced the overall signal-to-noise ratio and is not presented.

RESULTS AND DISCUSSION

We prepared binary azobenzene/alkane thiol SAMs of various fractions of azobenzene and observed their spectroscopic properties and isomerization kinetics with VSFG. Figure 1

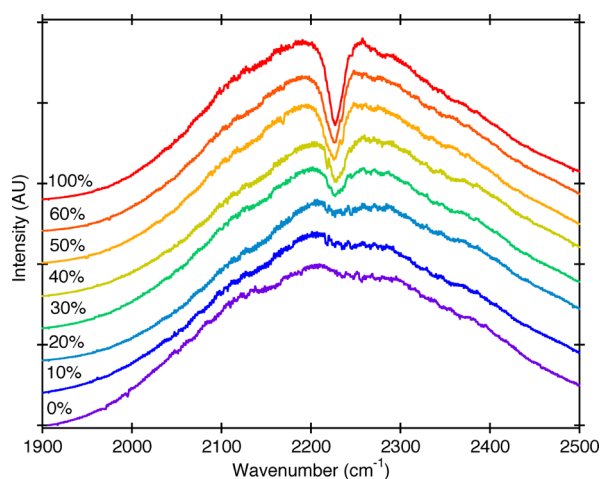


Figure 1. Normalized PPP-polarized SFG spectra from a set of different SAMs with percentage of azobenzene formulated SAMs. Spectral peak at 2220 cm^{-1} is from the nitrile group on the functionalized azobenzene. Broad background is the nonresonant SFG signal from gold.

shows the trend of the VSFG spectra for the PPP polarization in the nitrile stretch region ($\sim 2220 \text{ cm}^{-1}$) from samples formed with 100% alkane thiol SAM (zero solution volume percent azobenzene functionalized SAM) to neat (100%) azobenzene-functionalized SAMs. The nitrile stretch at 2224 cm^{-1} appears as a negative peak against the nonresonant background signal of the gold substrate. The peak's amplitude decreases as the azobenzene percentage in the precursor solution is reduced. A similar trend is observed in the SSP spectra presented in the Supporting Information.

VSFG provides the ability to quantitatively determine the concentration of a vibrational chromophore on a surface. Spectra are fit using the standard VSFG formalism,⁵² where the surface second-order nonlinear susceptibility $\chi^{(2)}$ is represented as a sum of a nonresonant term $\chi_{\text{NR}}^{(2)}$ describing the background signal from the gold surface and a resonant Lorentzian term $\chi_{\text{Res}}^{(2)}$ representing the nitrile vibrational resonance

$$\chi_{\text{NR}}^{(2)} = A_{\text{NR}} e^{i\phi} \quad (1)$$

$$\chi_{\text{Res}}^{(2)} = \frac{B_{\text{CN}}}{(\omega - \omega_{\text{CN}}) + i\Gamma} \quad (2)$$

for the total SFG signal intensity of $I_{\text{SFG}}(\omega) \propto |\chi_{\text{NR}}^{(2)} + \chi_{\text{Res}}^{(2)}|^2$. The shape of the nonresonant contribution was determined from the SFG signal off a reference clean Au substrate. Because the $\chi_{\text{Res}}^{(2)}$ signal is proportional to surface coverage of the nitrile chromophore, we can determine the surface fraction of azobenzene of different samples by fitting the amplitude B_{CN} of the resonant term. Figure 2 shows the correlation between

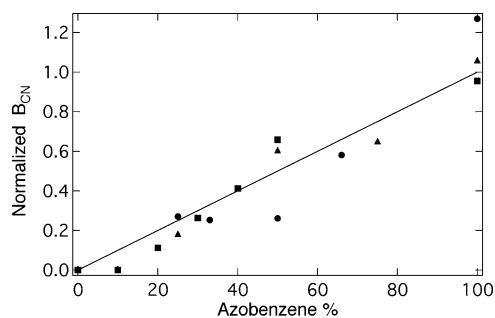


Figure 2. Amplitude B_{CN} of the resonant CN stretch signal in PPP-polarized VSFG spectra (normalized to linear relation) as a function of the solution fraction of azobenzene-functionalized precursor molecules used to form SAM. Different symbols correspond to different synthetic batches and experimental preparations of the SAMs.

the amplitude B_{CN} of the resonant signal $\chi_{\text{Res}}^{(2)}$ and the solution concentration of azobenzene-terminated thiol used to form the SAM. If the azobenzene-terminated thiol and alkane thiol had equal binding constants and noncooperative absorption then the amplitude of the resonant $\chi_{\text{Res}}^{(2)}$ signal of the nitrile marker would be directly proportional to the azobenzene mole fraction in precursor solution. While there may be a deviation from linear behavior at low azobenzene fractions (below 25%), possibly indicating the cooperativity in alkane thiol adsorption to exclude azobenzene-functionalized thiols, the correlation between B_{CN} and solution mole fraction is linear within the signal-to-noise at azobenzene fraction of 50% and above used in the measurements described below. We therefore assume that the azobenzene mole fraction in solutions used for SAM deposition represents the average surface coverage of the azobenzene thiols in the formed SAMs on the surface.

The ratio of nitrile signals taken at different SFG polarization combinations, PPP and SSP, can be used to determine the ensemble orientation. Figure 3 shows both the experimentally determined $\chi_{\text{PPP}}^{(2)}/\chi_{\text{SSP}}^{(2)}$ amplitude ratio for different azobenzene samples and the theoretical calculations described below. The experimental values in the left side of the panel were collected for PPP and SSP polarizations at six different dilutions of the azobenzene on the surface. The error bars shown account for the error in both the fitting of the $\chi_{\text{res}}^{(2)}$ amplitudes and the multiple measurements on the same azobenzene concentrations. Below 40% azobenzene concentration the relative error in the ratio is large primarily due to the low level of the $\chi_{\text{SSP}}^{(2)}$ signal. There appears to be a significant difference in the $\chi_{\text{PPP}}^{(2)}/\chi_{\text{SSP}}^{(2)}$ ratio measured for 100% and those of less than 100%, although, within error, the mixed SAMs do not exhibit significantly different response. The $\chi_{\text{PPP}}^{(2)}/\chi_{\text{SSP}}^{(2)}$ ratio for 100% is 21.5 ± 1.2 , and for <100% it is 18 ± 1.0 .

From these ratios we can obtain quantitatively the orientation of the nitrile moiety relative to the surface normal using a procedure developed by Zhuang et al.³⁶ This can be determined by comparing the ratios of the effective nonlinear susceptibilities

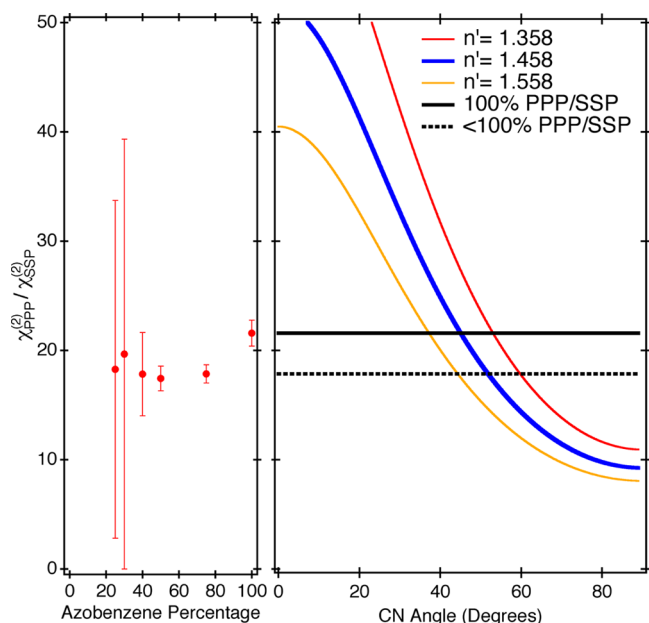


Figure 3. (Left) Calculated nitrile $\chi_{PPP}^{(2)}/\chi_{SSP}^{(2)}$ amplitude ratio for different ensemble angles of the nitrile moiety off of the surface normal. (Right) Experimental ratios for 100% and <100% azobenzene percentages compared to the theoretical $\chi_{PPP}^{(2)}/\chi_{SSP}^{(2)}$ for samples of different azobenzene percentages. Three values of n' graphed are bracketed around the index of bulk dodecane thiol of 1.458. Fit values are 37–53° for 100% azobenzene and 45–60° for <100% azobenzene.

$$\chi_{SSP}^{(2)} = \chi_{yyz} L_{yy}(\omega) L_{yy}(\omega_1) L_{zz}(\omega_2) \sin \alpha_2 \quad (3)$$

$$\begin{aligned} \chi_{PPP}^{(2)} = & -\chi_{xxz} L_{xx}(\omega) L_{xx}(\omega_1) L_{zz}(\omega_2) \cos \alpha \cos \alpha_1 \sin \alpha_2 \\ & - \chi_{zxx} L_{xx}(\omega) L_{zz}(\omega_1) L_{xx}(\omega_2) \cos \alpha \sin \alpha_1 \cos \alpha_2 \\ & + \chi_{zxx} L_{zz}(\omega) L_{xx}(\omega_1) L_{xx}(\omega_2) \sin \alpha \cos \alpha_1 \cos \alpha_2 \\ & + \chi_{zzz} L_{zz}(\omega) L_{zz}(\omega_1) L_{zz}(\omega_2) \sin \alpha \sin \alpha_1 \sin \alpha_2 \end{aligned} \quad (4)$$

There is only one nonzero $\chi^{(2)}$ tensor element contributing to the SSP and four elements for PPP given in eqs 5–7. The effective nonlinear susceptibilities are composed of three pieces. The trigonometric terms depend on the angles of incidence of the three beams: α for outgoing SFG, α_1 for visible, and α_2 for IR. The χ terms are the nonzero elements of the $\chi^{(2)}$ tensor for a vibrational chromophore of $C_{\infty v}$ point symmetry on an azimuthally isotropic surface³⁷

$$\chi_{xxz} = \chi_{yyz} = \frac{1}{2} N_s \beta [\cos \theta (1 + r) - \cos^3 \theta (1 - r)] \quad (5)$$

$$\chi_{zxx} = \chi_{zxx} = \frac{1}{2} N_s \beta [\cos \theta - \cos^3 \theta (1 - r)] \quad (6)$$

$$\chi_{zzz} = N_s \beta [r \cos \theta + \cos^3 \theta (1 - r)] \quad (7)$$

Here r is the ratio of molecular hyperpolarizability tensor elements; for chromophores of cylindrical symmetry around the c axis, $r = (\beta_{aaa}/\beta_{ccc}) = (\beta_{aaa}/\beta_{ccc})$. The value $r = 0.26$ was used for the nitrile moiety, in agreement with literature.³⁶ The tilt angle of the moiety from surface normal is represented by θ , assuming a δ -function distribution, and $N_s \beta$, a scaling constant, which cancels out upon taking a ratio.

The “ L ” terms are the Fresnel factors in eqs 8–10, which depend on the light frequency. These are derived using a three-layer model with the index of the two stacked layers, n_1 and n_2 , as well as the index of the monolayer represented by n' .³⁶

$$L_{xx}(\omega) = \frac{2n_1(\omega) \cos \gamma}{n_1(\omega) \cos \gamma + n_2(\omega) \cos \alpha} \quad (8)$$

$$L_{yy}(\omega) = \frac{2n_1(\omega) \cos \alpha}{n_1(\omega) \cos \alpha + n_2(\omega) \cos \gamma} \quad (9)$$

$$L_{zz}(\omega) = \frac{2n_2(\omega) \cos \alpha}{n_1(\omega) \cos \gamma + n_2(\omega) \cos \alpha} \left(\frac{n_1(\omega)}{n'(\omega)} \right)^2 \quad (10)$$

The refractive index values used were $n_{\text{air}} = 1$ for all wavelength values and $n_{\text{Au}} = 0.16 + 3.55i$ at 675 nm, $n_{\text{Au}} = 0.18 + 5.11i$ at 800 nm, and $n_{\text{Au}} = 2.66 + 31.55i$ at 4500 nm from the *Palik Handbook of Optical Constants of Solids*.⁵³ The effective index of the interfacial layer n' was taken to be 1.458, the index of bulk dodecane thiol.

On the right-hand side of Figure 3, the calculated $\chi_{PPP}^{(2)}/\chi_{SSP}^{(2)}$ ratio is plotted for tilt angle θ values between 0° and 90° from surface normal. The ratio is calculated for three values of n' (1.358, 1.458, and 1.558) to show how differences in the index of the monolayer affect the estimated fit angle of the nitrile. As a result of this procedure, we can bracket a range of orientational angles of the nitrile. For 100% azobenzene $\theta = 37$ –53° and for <100% from $\theta = 45$ ° to 60°. Others have reported orientational analysis on different *trans*-azobenzene SAMs using NEXAFS and quantitative XPS methods^{24,25} in qualitative agreement with our study.

We also recorded the VSG spectra in the 2900 cm^{-1} region corresponding to the C–H stretch vibrations of the saturated alkane chains. The primary sources of signal in this region are the terminal CH_3 stretch vibrational modes of the alkane thiol and the CH_2 stretch vibrational modes of the alkane chain of both the alkane- and the azobenzene-functionalized thiols. In the PPP spectra shown in Figure 4, the primary peaks observed for the neat alkane thiol SAMs are usually assigned to the CH_3

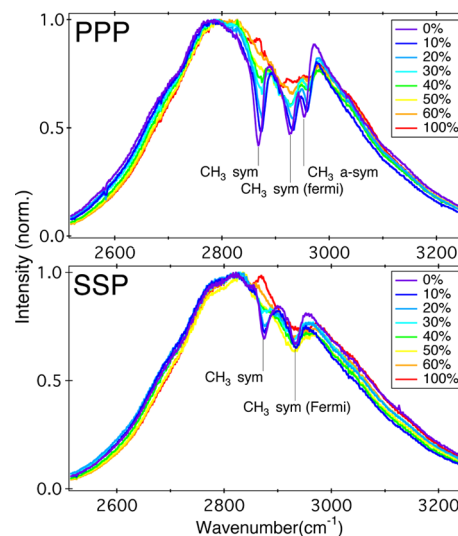


Figure 4. Normalized SFG spectra of PPP (top) and SSP (bottom) polarization of samples between 0% and 100% azobenzene-terminated C–H stretch modes.

symmetric stretch (2875 cm^{-1}), CH_3 asymmetric stretch (2968 cm^{-1}), and CH_3 Fermi resonance (2930 cm^{-1}) vibrational modes.^{33,40,54} In the SSP spectra, only the CH_3 symmetric (2875 cm^{-1}) and CH_3 Fermi resonance (2933 cm^{-1}) peaks are observed. This is consistent with previously reported SFG spectra for PPP and SSP polarization of well-ordered, vertically oriented alkane thiol SAMs.^{33,40,54} Underlying these peaks there are broader spectral features from the CH_2 modes of the alkyl chains^{33,35,41,51} which are present from the alkyl chains present in both the azobenzene-terminated thiol and the dodecane thiol. For the high azobenzene percentage films only CH_2 groups are observable. The qualitative trend observed with these peaks confirms the expected decrease of CH_3 signal of the alkane thiol as the solution percentage of azobenzene-terminated thiol increases. Due to the congestion of the CH -stretch spectral region, we did not use these spectra for isomerization studies. No appreciable changes were detected upon UV illumination.

■ ANALYSIS OF ISOMERIZATION

VSGF can be also used to monitor orientational changes of the nitrile marker upon azobenzene *trans* \rightarrow *cis* or *cis* \rightarrow *trans* isomerization. The magnitude and sign of the change in $\chi_{\text{Res}}^{(2)}$ upon isomerization of azobenzene are not trivial as they depend on the distribution of all three orientational Euler angles of the reactant *trans*-azobenzene, as detailed below. However, we were able to track in situ the $\chi^{(2)}$ resonant and nonresonant magnitudes as well as their relative phase upon exposure to UV light (340 nm, 4.5 mW/cm^2) to both quantify the magnitude of change upon isomerization and extract kinetic parameters for the monolayers. Figure 5 shows VSGF spectra of the nitrile

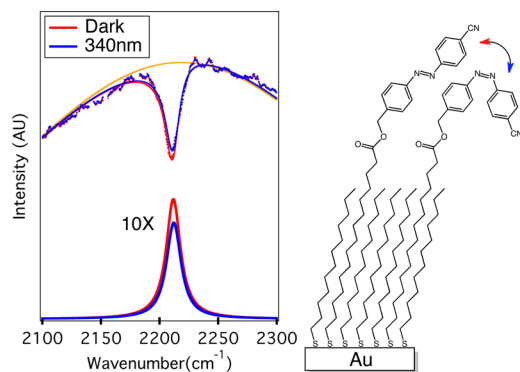


Figure 5. (Left) PPP SFG spectra for the nitrile stretch band of a 66% azobenzene film. Displayed are the experimental data for the film under 340 nm illumination (blue) and without (red). Spectra are fit with the nonresonant portion shown in yellow and the resonant portion shown on the bottom. (Right) Cartoon of mixed SAM on gold surface, formed from a mixture of azobenzene-functionalized thiol and dodecane thiol.

stretch band of a 66% azobenzene film prior to UV light exposure and during exposure to 340 nm light. Also shown is the decomposition of the spectrum into the Gaussian-shaped nonresonant signal $|\chi_{\text{NR}}^{(2)}|^2$ (yellow line) and the extracted resonant contribution intensity $|\chi_{\text{Res}}^{(2)}|^2$ (amplified by a factor of 10, red and blue lines on the bottom). There was little observed change of the nonresonant background $|\chi_{\text{NR}}^{(2)}|^2$ correlated with UV illumination. However, the resonant contribution, $\chi_{\text{Res}}^{(2)}$ shows a reproducible decrease of $\sim 10\%$ upon UV exposure.

Figure 6 shows the amplitude of the resonant SFG signal for the nitrile resonance for consecutive isomerization switching

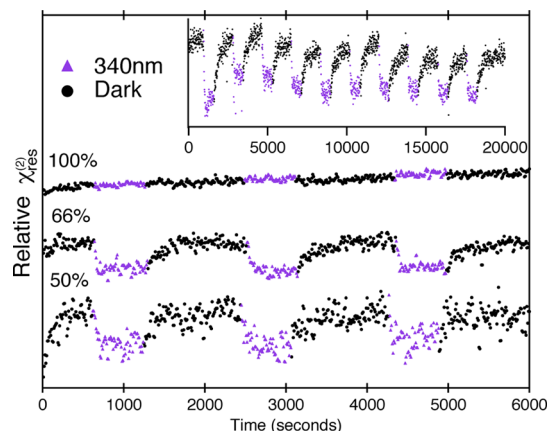


Figure 6. Change in the amplitude of nitrile $\chi_{\text{Res}}^{(2)}$ for 100%, 66%, and 50% azobenzene SAMs taken at 10 s intervals upon isomerization with 340 nm (10 min exposure, purple triangles) light and thermal relaxation in the dark (20 min periods, black circles). Inset shows 66% azobenzene SAM undergoing 10 concurrent isomerization cycles.

cycles alternating between 10 min exposures to 340 nm light and 20 min thermal relaxation in the dark for 100%, 66%, and 50% azobenzene samples. Up to 10 concurrent isomerization cycles were observed. Although the magnitude of change for the first cycle is somewhat larger than the concurrent cycles, repeated reversible isomerization steps can be performed with little observable decay in the magnitude of switching.

For the 50% and 66% samples, there is clearly observed isomerization with the total change of $\chi_{\text{Res}}^{(2)}$ of the nitrile marker of $\sim 10\%$ saturating at about 0.9 of the initial $\chi_{\text{Res}}^{(2)}$ amplitude of the all-*trans* state. Interestingly, for the 100% sample there is virtually no change of the resonant nitrile VSGF signal upon UV illumination. Only a very slight positive vertical offset, less than 1%, is observed which can be ascribed to some leakage of the UV lamp illumination detected by the CCD. Thus, we observe a nearly complete suppression of photoisomerization for a 100% azobenzene-functionalized SAM. The most likely explanation is steric hindrance by tightly packed azobenzene moieties which are all held at approximately the same height above the gold surface by the alkanethiol linker. Previous STM studies have shown tightly packed order in neat films of azobenzene-functionalized SAMs.¹² On the other hand, the alkanethiol spacers, which in our case are shorter than the azobenzene linkers (12 vs 15 carbons per chain, Figure 5), relieve the mutual congestion of the azobenzene head groups and allow isomerization to occur. Overall, the observation that pure azobenzene SAMs have hindered isomerization is consistent with the literature that postulates that at high packing fraction isomerization is hindered. This behavior has been assigned to both the intermolecular sterics^{30,55} and the delocalized excitonic coupling²⁴ at high densities to block *trans* \rightarrow *cis* isomerization.

■ ISOMERIZATION KINETICS

Figure 7 shows the kinetics of the $\chi_{\text{Res}}^{(2)}$ change due to *trans* \rightarrow *cis* photoisomerization upon UV illumination (top panel) and thermal *cis* \rightarrow *trans* recovery in the dark (bottom panel). Kinetic traces were obtained by averaging over several UV light exposure periods for the photoisomerization and dark periods

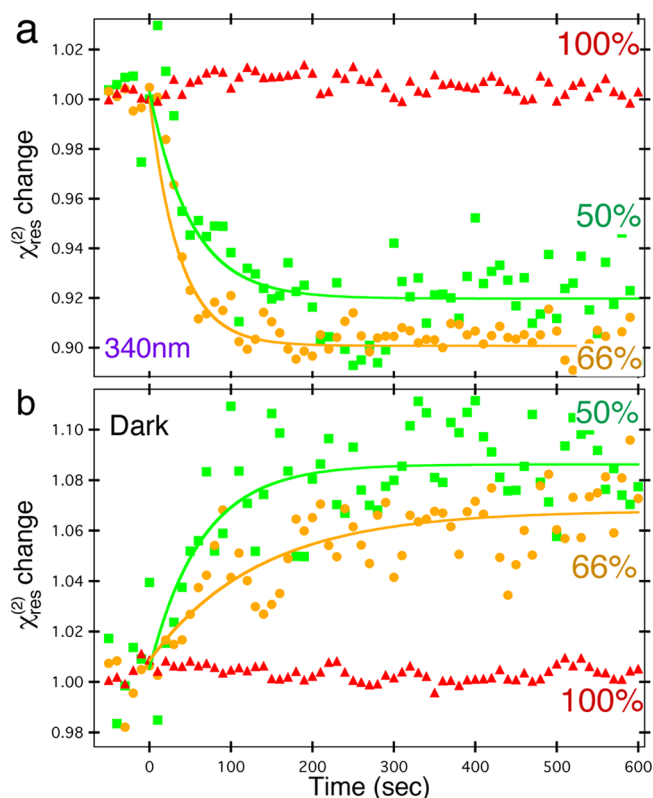


Figure 7. (A) Change in amplitude of the nitrile $\chi_{\text{Res}}^{(2)}$ under 340 nm illumination for 100%, 66%, and 50% azobenzene samples versus time. (B) Change in amplitude from the nitrile $\chi_{\text{Res}}^{(2)}$ for thermal relaxation in the dark following 10 min exposure to 340 nm light for 100%, 66%, and 50% azobenzene samples versus time. Data sets were averaged over multiple isomerization cycles. Solid lines show exponential fits described in the text.

for thermal recovery (Figure 6). The trans-to-cis photoisomerization kinetics can be fit by an exponential function of photon dose (n_p), $\Delta B_{\text{CN}}(n_p) = A(1 - e^{-\sigma_{\text{eff}} n_p})$. The fit of the kinetics under 340 nm illumination yields the effective photoisomerization cross-section $\sigma_{\text{eff}} = 2.3 \times 10^{-18} \text{ cm}^2$ for the SAM containing 50% azobenzene and $2.2 \times 10^{-18} \text{ cm}^2$ for 66% azobenzene SAM, which is comparable to literature values for similar azobenzene systems.^{27,49,56}

It is interesting to compare the trans \rightarrow cis photoisomerization quantum yield of azobenzene on the surface under 340 nm illumination to that in solution. For this comparison we assume that the absorption cross section of the surface-conjugated azobenzene is the same as that measured in the bulk. Taking the absorption cross section from solution at 340 nm of $4.81 \times 10^{-17} \text{ cm}^2$ ⁵⁷ and dividing by our measured photoisomerization cross section of $2.3 \times 10^{-18} \text{ cm}^2$ we get a quantum yield of isomerization for the dilute SAMs (50% or 66%) of $\sim 5\%$ (on average per photon per molecule), i.e., about one-half of the trans \rightarrow cis photoisomerization quantum yield following S_0 to S_2 excitation in solution, measured to be 11%.⁵⁷

The cis \rightarrow trans thermal isomerization kinetics can also be fit with a single exponential with a half-life of 49 s for 50% and 95 s for 66% azobenzene SAM. Although it is the subject of further ongoing investigations in our group, we note that the thermal recovery kinetics observed in SAMs on gold surfaces in this work are significantly faster than the cis \rightarrow trans thermal isomerization of azobenzene in solution which proceed on the time scale of many hours.⁵⁷

ISOMERIZATION MECHANISM

The magnitude of change in $\chi_{\text{Res}}^{(2)}$ signal upon isomerization can be modeled to derive more orientational information about the surface-bound azobenzene moieties. Some orientation models of the of azobenzene SAMs before and after isomerization exist in the literature. These are based on either geometrical arguments extrapolating from solution-phase fitting²⁶ or explicit ab initio simulation of azobenzene thiol cis configurations.⁵⁶ However, one of the difficulties in modeling isomerization is that the geometry of the cis-azobenzene isomer orientation inherently has more degrees of freedom than the trans isomer. Even a small distribution of orientational angles for the trans-azobenzene isomer therefore results in a bi- or trimodal distribution of orientational angles for the cis configuration after isomerization. Here we address two questions. First, we seek to quantify the isomerized fraction at saturation. Second, we want to determine if there is a preferential orientation of the resulting cis isomer relative to the surface.

The same theory used to determine the tilt angle of the nitrile moiety on the trans-azobenzene precursor can be used to construct a model to determine the expected change of VSG signal level upon isomerization from trans to various possible cis orientations. The model assumed an initial δ -function distribution in θ of the nitrile chromophore of the trans isomer. This, however, leaves uncertain the torsional orientation of the trans-azobenzene around the long axis of the molecule, i.e., the orientation of the $-\text{N}=\text{N}-$ bond relative to the surface normal (Figure 8). We approximate this uncertainty by assuming that upon isomerization the cis-azobenzene molecules assume two possible conformations: “Up” and “Down”. In the Up conformation, the nitrile group has rotated by 118° away from the plane of the surface, and in the Down conformation, the isomerization occurs toward the surface.⁵⁸ We consider three different scenarios: (1) assumes equal ratios of Up and Down conformations after isomerization (labeled Both in Figure 8); (2) assumes Up isomerization for 50% of the molecules while the remaining 50% are frozen in the trans form, e.g., as if Down isomerization is sterically hindered; (3) assumes only Down isomerization for 50% of the molecules with the remaining 50% frozen. While admittedly simplistic, this model should capture the essential bias in orientational changes upon isomerization. An alternative scenario of free torsional rotation is presented in the Supporting Information and yields similar results for the calculated change in $\chi_{\text{Res}}^{(2)}$ as scenario (1).

Equations 11–13 derive the expected relative change in $\chi_{\text{Res}}^{(2)}$ signal for PPP polarization (i.e., the ratio of $\chi_{\text{Res}}^{(2)}$ amplitude after isomerization to that of the all-trans monolayer before isomerization) as a function of the initial trans tilt angle θ and the fraction of isomerized molecules at saturation η . The first equation for $\chi_{\text{Both}}^{(2)}/\chi_{\text{Trans}}^{(2)}$ describes scenario 1 that starts with an orientation θ and after isomerization goes to equal contributions of both $\theta + 118^\circ$ and $\theta - 118^\circ$. The second equation for $\chi_{\text{Up}}^{(2)}/\chi_{\text{Trans}}^{(2)}$ only allows Up isomerization for one-half of the molecules while locking the orientation for the downward isomerizing azobenzenes. The last equation for $\chi_{\text{Down}}^{(2)}/\chi_{\text{Trans}}^{(2)}$ does the reverse, allowing only Down isomerization for one-half of the molecules. The $\chi_{\text{PPP}}^{(2)}(\theta)$ dependence is evaluated using eqs 4–7. For these calculations the effective index of the substrate, n' , value used was 1.458, although nearly all of the n' dependence cancels when solving for a change in signal.

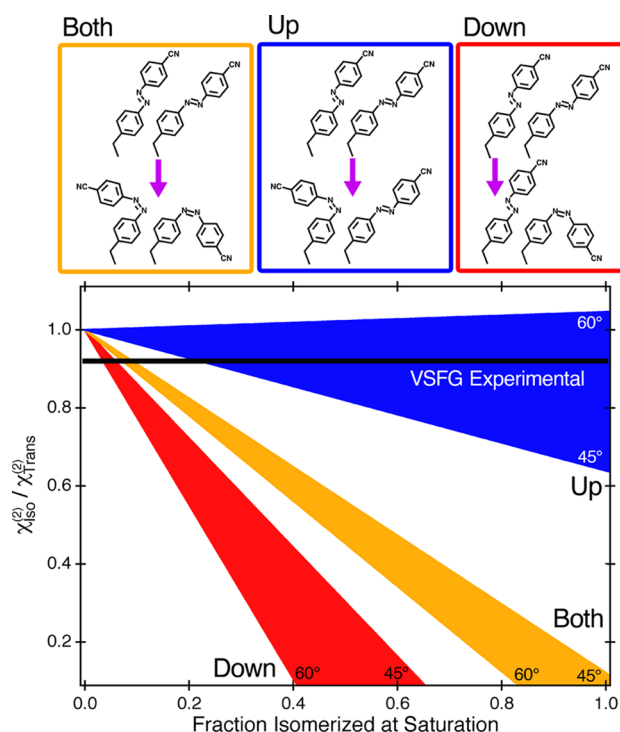


Figure 8. Three different scenarios for isomerization used: (1) where isomerization yields equal amounts of Up and Down states, (2) where only the Up states are free to isomerize, (3) where only the Down molecules can isomerize. The three cones (Both, orange; Up, blue; Down, red) map out the expected $\chi_{\text{Res}}^{(2)}$ change upon UV exposure for the three models as a function of isomerization fraction at saturation. Cones represent the range of tilt angles $\theta = 45\text{--}60^\circ$ of the trans isomer derived above (3). Black horizontal bar represents the experimentally observed value of $\Delta\chi_{\text{Res}}^{(2)}$ upon isomerization, 0.91.

$$\frac{\chi_{\text{Both}}^{(2)}(\theta, \eta)}{\chi_{\text{Trans}}^{(2)}} = \frac{\left| (1 - \eta)\chi_{\text{PPP}}^{(2)}(\theta) + \frac{\eta}{2}\chi_{\text{PPP}}^{(2)}(\theta + 118^\circ) + \frac{\eta}{2}\chi_{\text{PPP}}^{(2)}(\theta - 118^\circ) \right|}{|\chi_{\text{PPP}}^{(2)}(\theta)|} \quad (11)$$

$$\frac{\chi_{\text{Up}}^{(2)}(\theta, \eta)}{\chi_{\text{Trans}}^{(2)}} = \frac{\left| (1 - \eta)\chi_{\text{PPP}}^{(2)}(\theta) + \frac{\eta}{2}\chi_{\text{PPP}}^{(2)}(\theta + 118^\circ) + \frac{\eta}{2}\chi_{\text{PPP}}^{(2)}(\theta) \right|}{|\chi_{\text{PPP}}^{(2)}(\theta)|} \quad (12)$$

$$\frac{\chi_{\text{Down}}^{(2)}(\theta, \eta)}{\chi_{\text{Trans}}^{(2)}} = \frac{\left| (1 - \eta)\chi_{\text{PPP}}^{(2)}(\theta) + \frac{\eta}{2}\chi_{\text{PPP}}^{(2)}(\theta) + \frac{\eta}{2}\chi_{\text{PPP}}^{(2)}(\theta - 118^\circ) \right|}{|\chi_{\text{PPP}}^{(2)}(\theta)|} \quad (13)$$

Figure 8 shows the solutions for eqs 11–13 for θ angles within the $45\text{--}60^\circ$ range derived above (Figure 3). The observed experimental value is 0.91 $\chi_{\text{Res}}^{(2)}$ modulation upon isomerization, indicated by the horizontal black bar. Each cone represents the calculated values with regard to starting

orientation and fraction of isomerized molecules η for different scenarios: (1) Both (Orange), (2) Up (Blue), and (3) Down (Red). Although in these calculations the error introduced by the assumed n' value is small, the uncertainty in the θ value shown in Figure 3 remains. Our analysis allows for several possible mechanisms of isomerization. If there is little preference between the Up and the Down cis states, then the fraction of isomerized molecules at saturation must be very low ($<10\%$). This would be possible, for example, if phase segregation occurs between the azobenzene and alkane thiol spacers and isomerization occurs only at the edges of azobenzene domains. Another possibility suggested by Figure 8 is that a large fraction of molecules undergoes isomerization but the Up conformation is strongly preferred over the Down configuration, e.g., due to steric constraint for the Down configuration. This would result in a strong orientational preference of the cis-Up conformation over the cis-Down conformation after UV exposure. Since the model assumes 50% of the molecules undergoing Up mechanism isomerization, this is consistent with the measured quantum yield of 5% (per molecule per photon) in the monolayer on the surface being approximately one-half of that in solution (11%). Other studies have also seen a high-isomerization fraction for similar binary azobenzene SAMs.^{8,9}

CONCLUSIONS

We synthesized and characterized a novel azobenzene-functionalized SAM. Use of the same surface attachment chemistry as in regular thiol SAMs on gold surfaces allows us to prepare mixed monolayers where the azobenzene moieties are interspersed with shorter alkanethiol spacers. This approach enables investigation of mechanistic features of isomerization such as steric hindrance effects due to packing. Using VSG spectroscopy of the nitrile marker attached to the azobenzene moiety, we were able to observe the spectral modes of SAMs of a binary composition of the azobenzene-functionalized and alkylated thiols and quantitatively determine the relative surface coverage in mixed SAMs. Using the polarization-dependent VSG measurements of the nitrile signal we were able to quantitatively determine molecular orientation relative to the surface normal for different dilutions of the binary SAM.

VSG is sensitive to the orientational changes of the azobenzene moiety upon isomerization. Over 10 cycles of reversible isomerization were observed for dilute azobenzene-functionalized films. VSG also allows measurements of the photon dose required for photoisomerization from trans to cis conformation and thermal relaxation rates back to trans. We observe a pronounced steric hindrance of photoisomerization: no conformational change occurs upon UV illumination in neat (100%) azobenzene films, presumably due to tight packing of the headgroups limiting the conformational mobility or through excitonic coupling at high chromophore densities. However, photoisomerization and thermal recovery proceed and are reversible over multiple cycles when the azobenzene fraction is lowered to 66% or 50% (i.e., for as little as 34% of the shorter alkanethiol spacer). Perhaps this can be rationalized by the large amount of excess energy deposited into the azobenzene moiety upon 340 nm UV excitation into the S_2 state (likely, over an eV above the curve crossing that leads to either the cis or the trans ground state conformation^{59,60}). Lastly, orientational modeling of the VSG signals allows us to propose several possible isomerization mechanisms. The change of the VSG signal level upon UV exposure indicates

that a significant fraction of the azobenzene molecules isomerize with a cis conformation pointing away from the surface strongly preferred. We hope that this work will help increase the understanding of the isomerization mechanism by highlighting the importance of steric effects, packing, and crystallinity on the switching in dense films of actively isomeric molecules with either azobenzene functionality or other molecular switches that involve conformational change.

■ ASSOCIATED CONTENT

Supporting Information

This material is available free of charge via the Internet at <http://pubs.acs.org>.

■ AUTHOR INFORMATION

Corresponding Author

*E-mail: alex.benderskii@usc.edu.

Notes

The authors declare no competing financial interest.

■ ACKNOWLEDGMENTS

This research was supported by AFOSR Grant No. FA9550-09-1-0547. We thank Barry C. Thompson, Travis J. Williams, Dana Mustafa, and Janet Olson for discussions and help with organic synthesis. M.O. was supported as a summer undergraduate researcher by NSF REU grant CHE-0552397.

■ REFERENCES

- (1) Browne, W. R.; Feringa, B. L. *Annu. Rev. Phys. Chem.* **2009**, *60*, 407–428.
- (2) Liu, Z.; Hashimoto, K.; Fujishima, A. *Nature* **1990**, *347*, 658–660.
- (3) Ichimura, K.; Oh, S.; Nakagawa, M. *Science* **2000**, *288*, 1624–1626.
- (4) Delorme, N.; Bardeau, J.; Bulou, A.; Poncin-Epaillard, F. *Langmuir* **2005**, *21*, 12278–12282.
- (5) Ichimura, K.; Y, S.; Seki, T.; Hosoki, A.; Aoki, K. *Langmuir* **1988**, *4*, 1214–1216.
- (6) Zhang, C.; Du, M.; Cheng, H.; Zhang, X.; Roitberg, A.; Krause, J. *Phys. Rev. Lett.* **2004**, *92*, 158301.
- (7) Mativetsky, J. M.; Pace, G.; Elbing, M.; Rampi, M. A.; Mayor, M.; Samori, P. *J. Am. Chem. Soc.* **2008**, *130*, 9192D9193.
- (8) Kumar, A. S.; Ye, T.; Takami, T.; Yu, B.-C.; Flatt, A. K.; Tour, J. M.; Weiss, P. S. *Nano Lett.* **2008**, *8*, 1644–1648.
- (9) Zheng, Y. B.; Payton, J. L.; Chung, C.-H.; Liu, R.; Cheunkar, S.; Pathem, B. K.; Yang, Y.; Jensen, L.; Weiss, P. S. *Nano Lett.* **2011**, *11*, 3447–3452.
- (10) Katsonis, N.; Lubomska, M.; Pollard, M. M.; Feringa, B. L.; Rudolf, P. *Prog. Surf. Sci.* **2007**, *82*, 407–434.
- (11) Love, J.; Estroff, L.; Kriebel, J.; Nuzzo, R.; Whitesides, G. *Chem. Rev.* **2005**, *105*, 1103–1169.
- (12) Wolf, H.; Ringsdorf, H.; Delamarche, E.; Takami, T.; Kang, H.; Michel, B.; Gerber, C.; Jaschke, M.; Butt, H.; Bamberg, E. *J. Phys. Chem.* **1995**, *99*, 7102–7107.
- (13) Tamada, K.; Nagasawa, J.; Nakanishi, F.; Abe, K.; Ishida, T.; Hara, M.; Knoll, W. *Langmuir* **1998**, *14*, 3264–3271.
- (14) Zhang, J.; Whitesell, J.; Fox, M. *Chem. Mater.* **2001**, *13*, 2323–2331.
- (15) Dietrich, P.; Michalik, F.; Schmidt, R.; Gahl, C.; Mao, G.; Breusing, M.; Raschke, M. B.; Prievisch, B.; Elsaesser, T.; Mendelsohn, R.; Weinelt, M.; Rueck-Braun, K. *Appl. Phys. A: Mater. Sci. Process.* **2008**, *93*, 285–292.
- (16) Ulman, A. *Chem. Rev.* **1996**, *96*, 1533–1554.
- (17) Bordenyuk, A. N.; Weeraman, C.; Yatawara, A.; Jayathilake, H. D.; Stipokin, I.; Liu, Y.; Benderskii, A. V. *J. Phys. Chem. C* **2007**, *111*, 8925–8933.
- (18) Imabayashi, S.; Hobara, D.; Kakiuchi, T.; Knoll, W. *Langmuir* **1997**, *13*, 4502–4504.
- (19) Lee, L. Y. S.; Sutherland, T. C.; Rucareanu, S.; Lennox, R. B. *Langmuir* **2006**, *22*, 4438–4444.
- (20) Atre, S. V.; Liedberg, B.; Allara, D. L. *Langmuir* **1995**, *11*, 3882–3893.
- (21) Kakiuchi, T.; Iida, M.; Gon, N.; Hobara, D.; Imabayashi, S.; Niki, K. *Langmuir* **2001**, *17*, 1599–1603.
- (22) Nelson, K. E.; Gamble, L.; Jung, L. S.; Boeckl, M. S.; Naeemi, E.; Golledge, S. L.; Sasaki, T.; Castner, D. G.; Campbell, C. T.; Stayton, P. S. *Langmuir* **2001**, *17*, 2807–2816.
- (23) Jung, U.; Filinova, O.; Kuhn, S.; Zargarani, D.; Bornholdt, C.; Herges, R.; Magnussen, O. *Langmuir* **2010**, *26*, 13913–13923.
- (24) Gahl, C.; Schmidt, R.; Brete, D.; McNellis, E. R.; Freyer, W.; Carley, R.; Reuter, K.; Weinelt, M. *J. Am. Chem. Soc.* **2010**, *132*, 1831–1838.
- (25) Brete, D.; Przyrembel, D.; Eickhoff, C.; Carley, R.; Freyer, W.; Reuter, K.; Gahl, C.; Weinelt, M. *J. Phys.: Condens. Matter* **2012**, *24*, 394015.
- (26) Tamada, K.; Akiyama, H.; Wei, T. *Langmuir* **2002**, *18*, 5239–5246.
- (27) Tamada, K.; Akiyama, H.; Wei, T.-X.; Kim, S.-A. *Langmuir* **2003**, *19*, 2306–2312.
- (28) Campbell, D. J.; Herr, B. R.; Hulteen, J. C.; VanDuyne, R. P.; Mirkin, C. A. *J. Am. Chem. Soc.* **1996**, *118*, 10211–10219.
- (29) Walter, D. G.; Campbell, D. J.; Mirkin, C. A. *J. Phys. Chem. B* **1999**, *103*, 402–405.
- (30) Jeoung, E.; Rotello, V. M. *J. Supramol. Chem.* **2002**, *2*, 53–55.
- (31) Manna, A.; Chen, P.; Akiyama, H.; Wei, T.; Tamada, K.; Knoll, W. *Chem. Mater.* **2003**, *15*, 20–28.
- (32) Voges, A. B.; Al-Abadleh, H. A.; Musorriti, M. J.; Bertin, P. A.; Nguyen, S. T.; Geiger, F. M. *J. Phys. Chem. B* **2004**, *108*, 18675–18682.
- (33) Buck, M.; Himmelhaus, M. *J. Vac. Sci. Technol. A: Vac. Surf. Films* **2001**, *19*, 2717–2736.
- (34) Kim, J.; Somorjai, G. A. *J. Am. Chem. Soc.* **2003**, *125*, 3150–3158.
- (35) Bordenyuk, A. N.; Jayathilake, H.; Benderskii, A. V. *J. Phys. Chem. B* **2005**, *109*, 15941–15949.
- (36) Zhuang, X.; Miranda, P. B.; Kim, D.; Shen, Y. R. *Phys. Rev. B* **1999**, *59*, 12632–12640.
- (37) Wang, H. F.; Gan, W.; Lu, R.; Rao, Y.; Wu, B. H. *Int. Rev. Phys. Chem.* **2005**, *24*, 191–256.
- (38) Guyot-Sionnest, P.; Hunt, J. H.; Shen, Y. R. *Phys. Rev. Lett.* **1987**, *59*, 1597–1600.
- (39) Weeraman, C.; Yatawara, A. K.; Bordenyuk, A. N.; Benderskii, A. V. *J. Am. Chem. Soc.* **2006**, *128*, 14244–14245.
- (40) Nishi, N.; Hobara, D.; Yamamoto, M.; Kakiuchi, T. *J. Chem. Phys.* **2003**, *118*, 1904–1911.
- (41) Jayathilake, H. D.; Driscoll, J. A.; Bordenyuk, A. N.; Wu, L.; da Rocha, S. R. P.; Verani, C. N.; Benderskii, A. V. *Langmuir* **2009**, *25*, 6880–6886.
- (42) Walter, S. R.; Geiger, F. M. *J. Phys. Chem. Lett.* **2010**, *1*, 9–15.
- (43) Funk, S.; Bonn, M.; Denzler, D.; Hess, C.; Wolf, M.; Ertl, G. *J. Chem. Phys.* **2000**, *112*, 9888–9897.
- (44) Carter, J. A.; Wang, Z.; Fujiwara, H.; Dlott, D. D. *J. Phys. Chem. A* **2009**, *113*, 12105–12114.
- (45) Oh-e, M.; Tabe, Y.; Yokoyama, H. *Phys. Rev. E* **2003**, *68*, 061602.
- (46) Ohe, C.; Arai, M.; Kamijo, H.; Adachi, M.; Miyazawa, H.; Itoh, K.; Seki, T. *J. Phys. Chem. C* **2008**, *112*, 6359–6365.
- (47) Ohe, C.; Kamijo, H.; Arai, M.; Adachi, M.; Miyazawa, H.; Itoh, K.; Seki, T. *J. Phys. Chem. C* **2008**, *112*, 172–181.
- (48) Backus, E. H. G.; Kuiper, J. M.; Engberts, J. B. F. N.; Poolman, B.; Bonn, M. *J. Phys. Chem. B* **2011**, *115*, 2294–2302.
- (49) Wagner, S.; Leyssner, F.; Koerdel, C.; Zarwell, S.; Schmidt, R.; Weinelt, M.; Rueck-Braun, K.; Wolf, M.; Tegeder, P. *Phys. Chem. Chem. Phys.* **2009**, *11*, 6242–6248.
- (50) Prievisch, B.; Rueck-Braun, K. *J. Pept. Sci.* **2004**, *10*, 230.

- (51) Yatawara, A. K.; Tiruchinapally, G.; Bordenyuk, A. N.; Andreana, P. R.; Benderskii, A. V. *Langmuir* **2009**, *25*, 1901–1904.
- (52) Stiopkin, I. V.; Jayathilake, H. D.; Weeraman, C.; Benderskii, A. V. *J. Chem. Phys.* **2010**, *132*, 234503.
- (53) Palik, E.; Ghosh, G. *Handbook of Optical Constants of Solids*; Academic Press: New York, 1997; Vol. 3.
- (54) Zhang, H.; Baldelli, S. *J. Phys. Chem. B* **2006**, *110*, 24062–24069.
- (55) Yasuda, S.; Nakamura, T.; Matsumoto, M.; Shigekawa, H. *J. Am. Chem. Soc.* **2003**, *125*, 16430–16433.
- (56) Jung, U.; Schütt, C.; Filinova, O.; Kubitschke, J.; Herges, R.; Magnussen, O. *J. Phys. Chem. C* **2012**, *116*, 25943–25948.
- (57) Zimmerman, G.; Chow, L.; Paik, U. *J. Am. Chem. Soc.* **1958**, *80*, 3528–3531.
- (58) Eligehausen, S.; Sarge, S. M.; Öhlschläger, G.; Cammenga, H. K. *J. Therm. Anal. Calorim.* **1989**, *35*, 515–526.
- (59) Lednev, I.; Ye, T.; Hester, R.; Moore, J. *J. Phys. Chem.* **1996**, *100*, 13338–13341.
- (60) Fujino, T.; Arzhantsev, S.; Tahara, T. *J. Phys. Chem. A* **2001**, *105*, 8123–8129.